JOURNAL OF Applied Polymer SCIENCE

Toughening of Unmodified Polyvinylchloride Through the Addition of Nanoparticulate Calcium Carbonate and Titanate Coupling Agent

I. Kemal,[1,2] A. Whittle,[3] R. Burford,[2] T. Vodenitcharova,[1] M. Hoffman[1]

[1]School of Materials Science and Engineering, Faculty of Science, University of New South Wales, Sydney, New South Wales 2052, Australia

[2] School of Chemical Engineering, Faculty of Engineering, University of New South Wales, Sydney, New South Wales 2052, Australia

[3]IPLEX Pipelines Australia Pty Ltd., 35 Alfred Road, Sydney, New South Wales 2170, Australia

Correspondence to: M. Hoffman (E-mail: m.hoffman@unsw.edu.au)

ABSTRACT: PVC/$CaCO_3$ polymer nanocomposites of differing compositions were produced using a two-roll mill and compression molding. In all formulations, 0.6 phr of titanate was incorporated to assist dispersion during processing. The morphology was observed using transmission electron microscopy, and the static and dynamic mechanical and fracture properties were determined. Fracture toughness examination was performed according to strain energy release test method. The presence of nanometer-sized $CaCO_3$ particles led to a slight decrease in the tensile strength but improved the impact energy absorption, storage modulus, and fracture toughness. The use of titanate coupling agent softened the polymer matrix and reduced the matrix's modulus. Fracture surface examinations by scanning electron microscopy showed that the coupling agent improved particle–matrix bonding and inhibited void formation around the particles. Finite element analysis suggested that the improved particle–matrix bonding reduced the matrix's plasticity around the particles, which decreased the toughening efficiency of the composites. © 2012 Wiley Periodicals, Inc. J. Appl. Polym. Sci. 000: 000–000, 2012

KEYWORDS: PVC nanocomposite; titanate coupling agent; strain energy release rate; finite element analysis

Received 28 February 2011; accepted 22 March 2012; published online
DOI: 10.1002/app.37774

INTRODUCTION

From our previous study,[1] it was found that the addition of nano-$CaCO_3$ particles (NPCC) to a PVC matrix could simultaneously improve both fracture toughness and stiffness, which cannot be achieved by the traditional addition of impact modifiers to PVC, in which toughness increases but stiffness is sacrificed.[2] The toughness improvement of PVC reinforced with nanoparticles is believed to be due to the cavity formation at the particle–matrix interfaces, which releases plastic constraint allowing larger plastic deformation and hysteretic energy absorption processes at the crack tip.[3] Despite their advantages, development and commercialization of nanocomposite materials have been limited by difficulties in obtaining homogeneous dispersion of nanoparticles in the polymer matrix.[4]

Nanosized particles have a strong tendency to agglomerate because of their large surface area, and hence, surface energy. Interactions between particles are affected by the contributions of attraction and repulsion as a result of Van der Waals and electrostatic forces.[5,6] As the particle size decreases, the reduction in repulsive electrostatic forces is much more significant than the reduction in attraction because of the Van der Waals force, and therefore, the attraction dominates the interface and results in particle agglomeration.[5,6]

The agglomeration gives stability, which is beneficial during transportation and particle handling. On the other hand, the agglomerates create a problem, as it can be very difficult to disperse the nanosized particles in the polymer matrix. Most filler particle manufacturers try to overcome this problem by coating the particle surface with low-cost surfactants, such as stearic acid, to improve filler incorporation and dispersion by minimizing interparticle interaction and improving particle–matrix interaction.[7,8]

Surfactant, such as stearic acid, works by preferential adsorption of the polar group to the particle surface by electrostatic interaction. An electron spectroscopy study (ESCA) carried out on

Additional Supporting Information may be found in the online version of this article.

the surface of $CaCO_3$ by Fekete et al.[9] has shown an ionic bond formation between the surfactant molecules and the filler surface. Nevertheless, agglomeration still occurs for treated $CaCO_3$, as the interparticle attraction is beyond the separating force of the surfactants.

A stronger particle–matrix interaction can be provided by the surface treatment of the particles through chemical reaction with a coupling agent. Coupling agents are additives consisting of bifunctional molecules, which are able to chemically bond two dissimilar substrates.[7] Coupling agents not only aid the mixing of two phases but also help to improve the particle dispersion by making the surfaces of the particle more hydrophobic and enabling the elimination of water from hydration and air voids, resulting in deagglomeration.[7,10]

Different types of coupling agent, such as silane, titanate, zirconate, and polymeric-based agents, have been used to combine different interfaces for many decades.[7] In the case of PVC/$CaCO_3$ particles composite system, a titanate-based coupling agent has been more successful in providing chemical bonding and dispersion. The molecular formula is described as XO-Ti-$(OY)_3$, where XO— is the alkoxy group capable of reacting with the inorganic substrate, and —OY is the organofunctional fragment.[11] The Y portion can typically contain several different groups to provide interaction with polar and nonpolar thermoplastics (e.g., benzyl and butyl) and thermosets (e.g., amino and methacryl) as well as binder groups such as pyrophosphato or carboxyl, which can introduce additional functions to the composite.[11] Silane provides chemical coupling by reaction with oxide or hydroxyl group available on the particle surface, which are not available on the surface of $CaCO_3$ particles.[10] On the other hand, titanate reacts with the surface protons through solvolysis or coordination without the need of water condensation, thus creating a monomolecular layer on the organic surface that can react with an organic polymer.[11] As a result, titanate can be used to couple interfaces that are nonreactive with silane, including calcium carbonate.[10,11]

Titanate-based coupling agents have been used in a number of research studies, demonstrating improved particle–matrix bonding and nanosized particles dispersion.[12] Furthermore, the titanate coupling agents also act as plasticizers,[13] which can facilitate higher filler loadings,[14] and as a catalyst for a number of reactions in the polymer matrix. Most researchers pretreat the NPCC with titanate either by directly spraying it onto the particles or by immersion of the NPCC in a solution containing the coupling agent.[12] This method, however, is time consuming and increases the cost of the fillers because of the extra processing. Another method widely used in the industry is blending the polymer, filler, and coupling agent before intensive mixing with other additives, followed by melt compounding.[7,10,15] This method is called *in situ* coupling.

Although titanate coupling agents can improve dispersion, the implications regarding the mechanical properties have not been thoroughly discussed. In the case of titanate pretreatment of the fillers, the tensile strength has been reported to show some improvement because of stronger bonding between the particles and the matrix[16]; nevertheless, the influence on the modulus, fracture toughness, and fracture mechanics is not yet clear.

In our previous study,[1] an impact-test method[17] was used to assess the fracture toughness, that is, the critical strain energy release rate G_c. It was found that in the case of PVC with untreated NPCC reinforcement, the G_c value increased with the volume fraction. At 20 phr NPCC, the G_c was found to be 5.03 kJ/m^2, exceeding the fracture toughness of m-PVC.[1] In this study, the same method was used to determine the fracture toughness of the composites, which were manufactured with the addition of titanate-based coupling agents.

In this study, we looked for ascertaining the changes in the particle dispersions, the mechanical properties, and the deformation mechanism associated with the *in situ* addition of titanate coupling agent into the PVC/nano-$CaCO_3$ composites. The results obtained were compared with our previous results,[1] in which the PVC nanocomposites were processed without coupling agent and the use of impact modifiers for toughness enhancement. PVC nanocomposites with differing NPCC fractions were processed by a melt-blending method, and a fixed amount of titanate coupling agent was directly added in each formulations. The microstructures of the composites were observed under transmission electron microscopy (TEM), and the extensive fracture surface analysis was performed to understand the deformation mechanism. Mechanical testing, including tensile testing, impact tests, dynamic mechanical analysis (DMA), and fracture toughness tests were performed to assess the effect of the coupling agent on the strength, toughness, and stiffness of the nanocomposites. A finite element-based model was then developed to demonstrate the effect of particle–matrix bonding strength on the deformation behavior of the nanocomposites.

EXPERIMENTAL PROCEDURES

Material Processing

Raw materials consisting of PVC resins (K57, Australian Vinyls, Laverton, Victoria, Australia) and Ca–Zn-based thermal stabilizers (CP 1009, Chemson Pacific, Eastern Creek, NSW, Australia) were mixed with the NPCC particles (NPCC, Singapore Nano Materials Technology, Singapore) at different volume fractions [3, 6, 9, 12, and 20 parts per hundred of resin (phr) by weight] through a dry-mixing process. The molecular weight and relative density of the PVC resins are approximately 140,000 and 1.45, respectively. A titanate coupling agent (CAPOW L38/H, Kenrich Petrochemical, Bayonne, New Jersey, USA) at 0.6 phr titanate was introduced to each dry blend formulation, including a monolithic PVC sample for reference. The 0.6 phr titanate dosage was based on the reference manual supplied with CAPOW L38/H, which suggested optimal dosage of 0.2–0.6 wt %.[18]

The PVC resin, NPCC filler, and titanate coupling agent were initially mixed to homogenize the particles and the coupling agent. A thermal stabilizer was added to the dry mix compound before further mixing. The two-stage mixing (integral blending) procedure was used in this study to maximize the distributions of titanate at the particle–resin interface. Dry mixing was carried out from room temperature to 82°C ($\sim$ 8 min) below the boiling point of the titanate coupling agent. The dry blend was cooled by mixing at room temperature for 2 min and then conditioned for a day at room temperature to remove moisture. The nanocomposites were compounded by a two-roll mill

operating at equal roll speeds and at a temperature of 175°C. The resulting compounds were cooled and granulated into flakes using a bench-top mechanical granulator. The flakes were then molded into rectangular sheets by compression molding at 185°C and 2 MPa pressure for 5 min using a Carver-type press.

Microstructural Characterization

The NPCC filler was characterized by TEM and the Image-J analysis software (NIH freeware) as per our previous work.[1] The NPCC TEM micrograph is shown in Supporting Information Figure S1, and the particle size distribution based on image analysis is shown in Supporting Information Figure S2. BET surface area measurement was used to calculate the surface area, using a Micromeritics Tristar 3000 Analyzer in a nitrogen environment. The particles were pretreated at 150°C under vacuum to remove moisture before BET measurement.

The morphology was observed under JEOL1400 TEM at an accelerating voltage of 75 kV. For this purpose, thin sections (~ 100 nm) of the composites were cut using a diamond knife-equipped Reichert Jung ultramicrotome at room temperature and placed on a formvar-coated copper grid for TEM observation. The nanoparticle dispersion was characterized by Image-J analysis software (NIH freeware) on the TEM micrographs. Examination of the fracture surfaces following mechanical testing was carried out using a JEOL S900 scanning electron microscope with a field emission gun (FESEM). The samples were coated with chromium metal before observation. To observe the crack process zone, a cross section perpendicular to the impact fracture plane was cut in the center along the notch. The surface was trimmed by ultramicrotome and coated with chromium before observation by FESEM.

Mechanical Testing

Six tensile dumbbells specimens of each composition were machined from the compression-molded slab using a pantograph cutting tool conforming to type 1 ISO R527 : 1966.[19] Tensile testing was undertaken according to AS1145.1-2001[20] using an Instron model 1185 universal tensile testing machine at an extension rate of 10 mm/min. The tensile elongation to break was measured using a laser extensometer.

DMA was carried out using a TA Instruments DMA Q800 with a three-point-bend dual cantilever configuration. The samples were 45 mm × 12 mm × 5 mm and cut from the compression-molded slab. The samples were heated from room temperature to 135°C, at 2°C per minute, cycling at 5 μm amplitude, and 1 Hz frequency.

A Charpy impact test was performed according to AS1146.2-1990[21] using a Zwick Model 5102 pendulum impact tester. For this test, 10 single-edge-notched beam (SENB) impact test specimens (100 mm × 12.7 mm × 5 mm) were cut from the compression-molded slab using a band saw and notched using a multitoothed broaching tool, as described in ISO/DIS 11673.2,[22] giving a notch radius of ~ 16 μm. Similarly, 22 SENB specimens of the same dimensions, but with different notch depths, were produced for fracture toughness testing. The notches were cut in the center of the bars to depths of ~ 0.8 to 7.0 mm, and the samples were conditioned at 20°C ± 2°C for 1 day. The

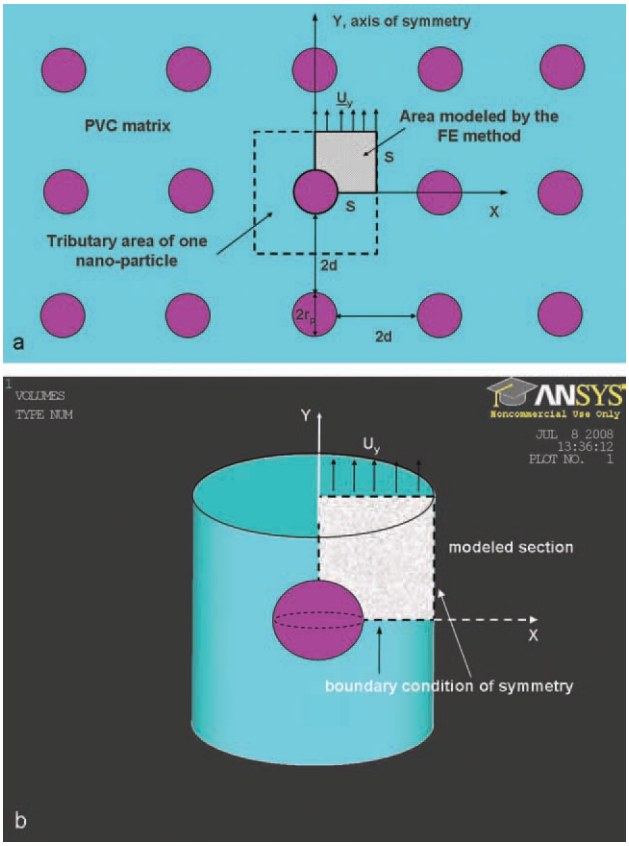

Figure 1. (a) Schematic of the FE model assuming homogeneous particles distribution in the matrix, and (b) modeled structure following application of axisymmetric constraints. [Color figure can be viewed in the online issue, which is available at wileyonlinelibrary.com.]

energy to fracture was measured at the point of impact on a pendulum impact tester using a 0.5-J hammer, with the support span set at 70 mm and the impact velocity set to 2.93 m/s. The fracture toughness of the composites was calculated according to the ESIS strain energy release rate protocol.[17]

Finite Element Analysis

Our previous study[1] found that debonding at a very weak particle–matrix interface led to cavitation. In this study, we considered the effect of interfacial strength, which was expected to be affected by the titanate coupling agent, and the subsequent cavity formation by using a finite element model. The analysis took into account two different scenarios of bonding strength: (i) moderate bonding and (ii) strong bonding (perfect bond). For both cases, the existence of the particles could not be ignored and had to be taken into consideration. Thus, one rigid $CaCO_3$ particle of radius r_p was incorporated in a 2D axisymmetric FEA model. The axisymmetric model enabled an accurate estimate of mechanical behavior in the vicinity of an inclusion as shown in the previous analysis.[1]

A schematic of the modeled structure, assuming a uniform particle distribution through the matrix, is shown in Figure 1(a), where S denotes symmetry boundary conditions, and $2d$ is the distance between two particles in both the x- and y-directions. A tensile strain was applied via a displacement in the y-direction

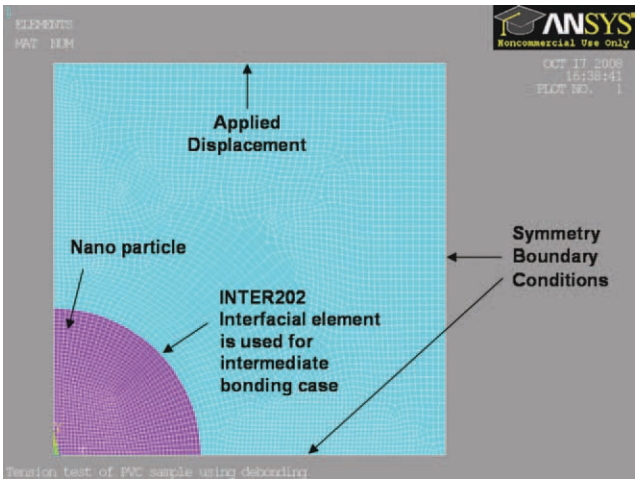

Figure 2. Two-dimensional FEA mesh of a rigid particle (purple color) and the surrounding matrix (light blue) with the interfacial layer modeled using INTER202 element. [Color figure can be viewed in the online issue, which is available at wileyonlinelibrary.com.]

U_y. The model covers the tributary volume of one nanoparticle of 20, 30, and 40 nm radius (r_p). It should be noted that the particle diameter alone is not significant for the FEA simulation; instead, the FEA simulation is based on the volume fraction, which is a function of the particle size and the interparticle distance. The effect of the particle was properly considered as the volume fraction in the FEA simulations was taken as the same as in the experiments. Axisymmetric conditions were then applied, as illustrated in Figure 1(b).

The FE Software ANSYS v11 was used. The model was meshed with PLANE182 2D linear solid elements using enhanced strain formulation (Figure 2). A mesh was generated with 60 element divisions along each line, which provided 5622 elements (Figure 2) and mesh-independent results.

The elastic modulus of the $CaCO_3$ particle was taken to be 35 GPa,[7] and the matrix modulus was taken to be 3440 MPa based on the experimental data. A multilinear deformation formulation was chosen for the matrix using the true tensile stress–strain curve of the u-PVC matrix, containing 0.6 phr titanate coupling agent (Figure 3). The true stress–strain was calculated from the engineering stress–strain curve according to the method of Du et al.[23] as shown in Figure 3. It was assumed that yielding of the matrix in uniaxial tension occurs at the maximum stress $\sigma_{m,y}$ (Figure 3), which was estimated to be 63.5 MPa. This stress is realized at a plastic strain of 2% (denoted by $\varepsilon^p_{m,y}$). Von Mises failure criterion was applied in this study, according to which the composites fail when the equivalent stress (σ^{eqv}_m) and equivalent plastic strain ($\varepsilon^{eqv,p}_m$) in the matrix satisfy the following:

$$\sigma^{eqv}_m = \sigma_{m,y}, \tag{1}$$

$$\varepsilon^{eqv,p}_m = \varepsilon^p_{m,y}, \tag{2}$$

where $\sigma_{m,y} = 63.6$ MPa and $\varepsilon^p_{m,y} = 2\%$, as mentioned above. The multilinear model was introduced in which the discrete values of stress and corresponding strain closely follow the experimental curve as shown by the hollow circles in Figure 3.

In the FEA model, the tension was applied in terms of applied displacement in the positive y-direction (U_y), which is the elongation of the sample, as shown in Figure 1(a). The induced tensile force (P) was then determined as the sum of the reaction forces in all the nodes pulled by U_y. The average applied stress and the applied strain on the composite (i.e., σ_c and ε_c) were then calculated as follows:

$$\sigma_c = \frac{P}{d + r_p}, \tag{3}$$

$$\varepsilon_c = \frac{U_y}{d + r_p}. \tag{4}$$

In the case of perfect (strong) bonding, interfacial delamination could not occur. However, when the interfacial adhesion was moderate, it was assumed that delamination was possible. Thus, to simulate the interface surfaces and the subsequent delamination process, a layer of 2D, four-node cohesive zone elements, INTER202, was incorporated into the 2D axisymmetric model (Figure 2). The separation was represented by an increasing displacement between nodes, within the interface element itself that were initially coincident. The cohesive elements in the FE model require the provision of the following parameters: a maximum normal stress at the interface σ_{max} [Figure 4(a)] and a normal separation δ_n [Figure 4(b)] across the interface, where the maximum normal stress is attained (Mode I debonding).

These parameters were chosen in the following way: the maximum normal stress was chosen to be the debonding strength and set to be the strength at which inelastic deformation was initiated according to the tensile testing of the composites,[24,25] that is, $\sigma_{max} = \sigma_{m,y}$.

Interfacial adhesion in the case of intermediate strength bonding was defined by the energy required to break the particle–matrix interface for a single particle given by[24,25]:

$$G_{ic,i} = \frac{3\sigma^2_{max} r_p}{4\pi E_m}, \tag{5}$$

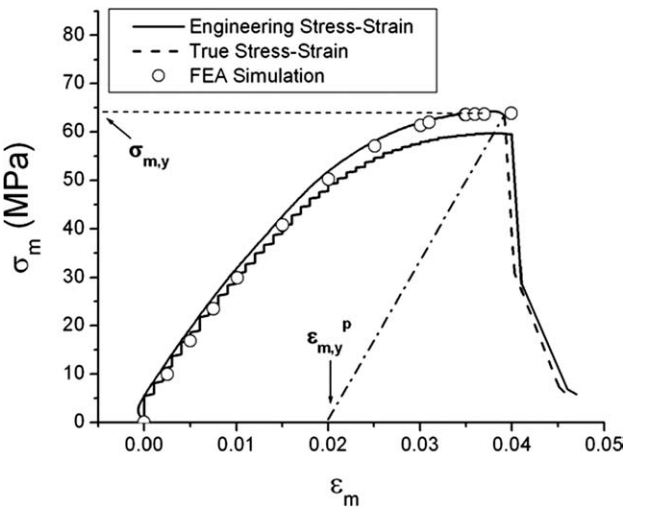

Figure 3. Engineering and true stress–strain curve of u-PVC processed with 0.6 phr titanate coupling agent.

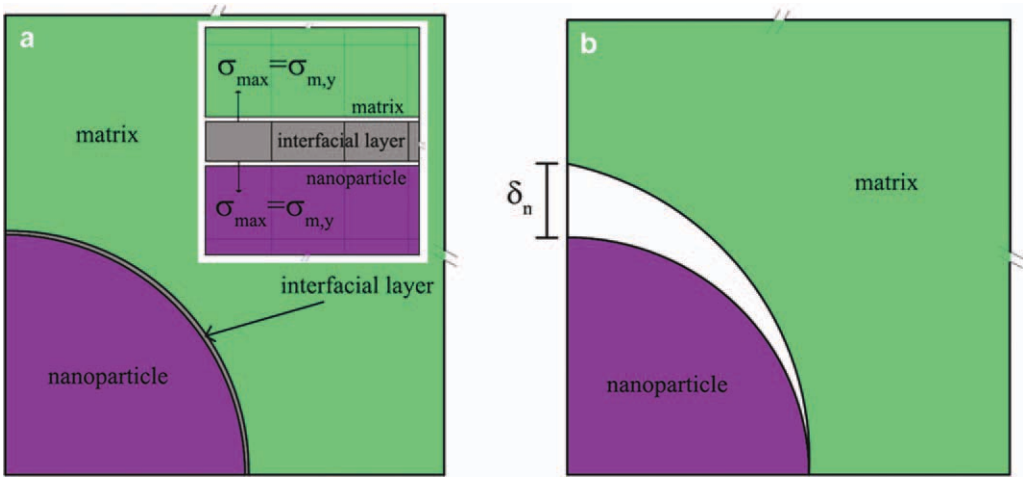

Figure 4. Illustration of (a) the maximum normal stress and (b) the normal separation at the cohesive interfacial element in the FE model. [Color figure can be viewed in the online issue, which is available at wileyonlinelibrary.com.]

where σ_{max} is the maximum stress normal to the interface required to initiate debonding, E_m is the matrix's modulus, and r_p is the radius of the particles. The applied tension and tensile strain on the composite at which debonding occurs are denoted by $\sigma_{c,d}$ and $\varepsilon_{c,d}$, respectively.

The debonding energy calculated using Eq. (5) was found to be 72.2×10^{-4} J, when taking $\sigma_{m,y} = 63.6$ MPa, $E_m = 4012.5$ MPa, and $r_p = 30$ nm. The energy was calculated from the area under the stress–displacement curve (Figure 5). Knowing the debonding stress (σ_{max}) and debonding energy ($G_{ic,i}$), the separation (δ_n) at debonding was calculated as $\delta_{n,y} = 2G_{ic,i}/\sigma_{m,y}$. To account for other possible debonding energies and to compare with the energy calculated from Eq. (5), another situation was considered, that is, debonding strength at 75% of the tensile yield strength ($\sigma_{m,y}$). Maintaining the same contact cohesive zone element stiffness K_n, the normal distance at debonding was calculated to be 75% of the normal distance, that is, $\delta_n = {}^3/_4\delta_{n,y}$ at $\sigma_{max} = {}^3/_4\sigma_{m,y}$.

For the u-PVC with a titanate coupling agent, the stress–strain curve (Figure 3) indicated that the yield point for the matrix in uniaxial tension was $\sigma_{m,y} = 63.6$ MPa. For both intermediate and perfect bonding cases, it was assumed that the composite yields when the matrix has yielded. Thus, the applied tensile stress on the composite at the onset of plasticity ($\sigma_{c,y}$) was determined to be at the loading step at which the equivalent stress in the matrix (σ_m^{eqv}) equals the value of $\sigma_{m,y} = 63.6$ MPa. Similarly, the applied strain in the composite ($\varepsilon_c = \varepsilon_{c,y}$) induces von Mises plastic strain at any point in the matrix (ε_m^p) equal to the plastic yield strain in the matrix of 2% in uniaxial tension, $\varepsilon_{m,y}^p = 2\%$.

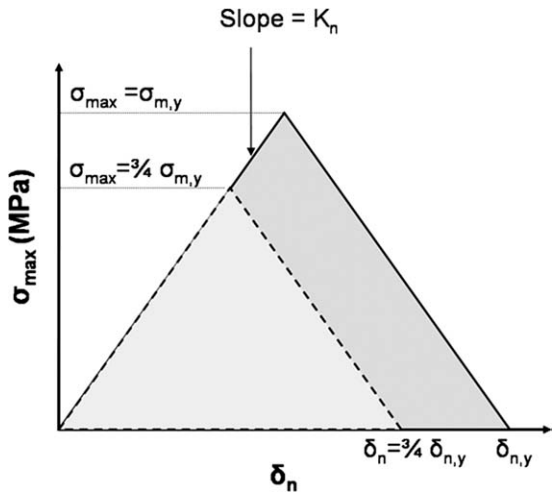

Figure 5. Stress–displacement curve representing the interfacial debonding energy.

RESULTS AND DISCUSSION

TEM micrograph of the NPCC used to reinforce the PVC and the particle size distribution can be seen in Ref. 1. The NPCC average particle size calculated by image analysis was found to be 60 ± 20 nm. BET surface area measurement found that the NPCC surface area was 24 m^2/g, which, assuming a spherical particle and density of 2.65 g/cm^3, gives an average particle size of 47 nm.[1]

The micrographs of the composites show the NPCC particles distributed homogeneously through the matrix [Figure 6(a–e)]. It can be seen that particle dispersion is homogeneous despite slight agglomerates at a higher volume fraction. This could be associated with the fact that there is insufficient titanate, as it was kept at 0.6 phr, to adequately couple the larger particle–matrix interfacial area, which increased with the particle volume fraction. The level of agglomeration, however, is much lower than that observed for composites without a coupling agent.[1] This is confirmed by image analysis using Image-J processing software on the TEM micrographs, indicating majority of particles size in the range of less than 100 nm (Figure 7). The homogeneous particle dispersion was facilitated by a combination of the coupling agent and the high levels of shear produced in the blend by the two-roll mill.

Mechanical Properties

The tensile strength was found to decrease with increasing NPCC content (Figure 8). The method of characterizing

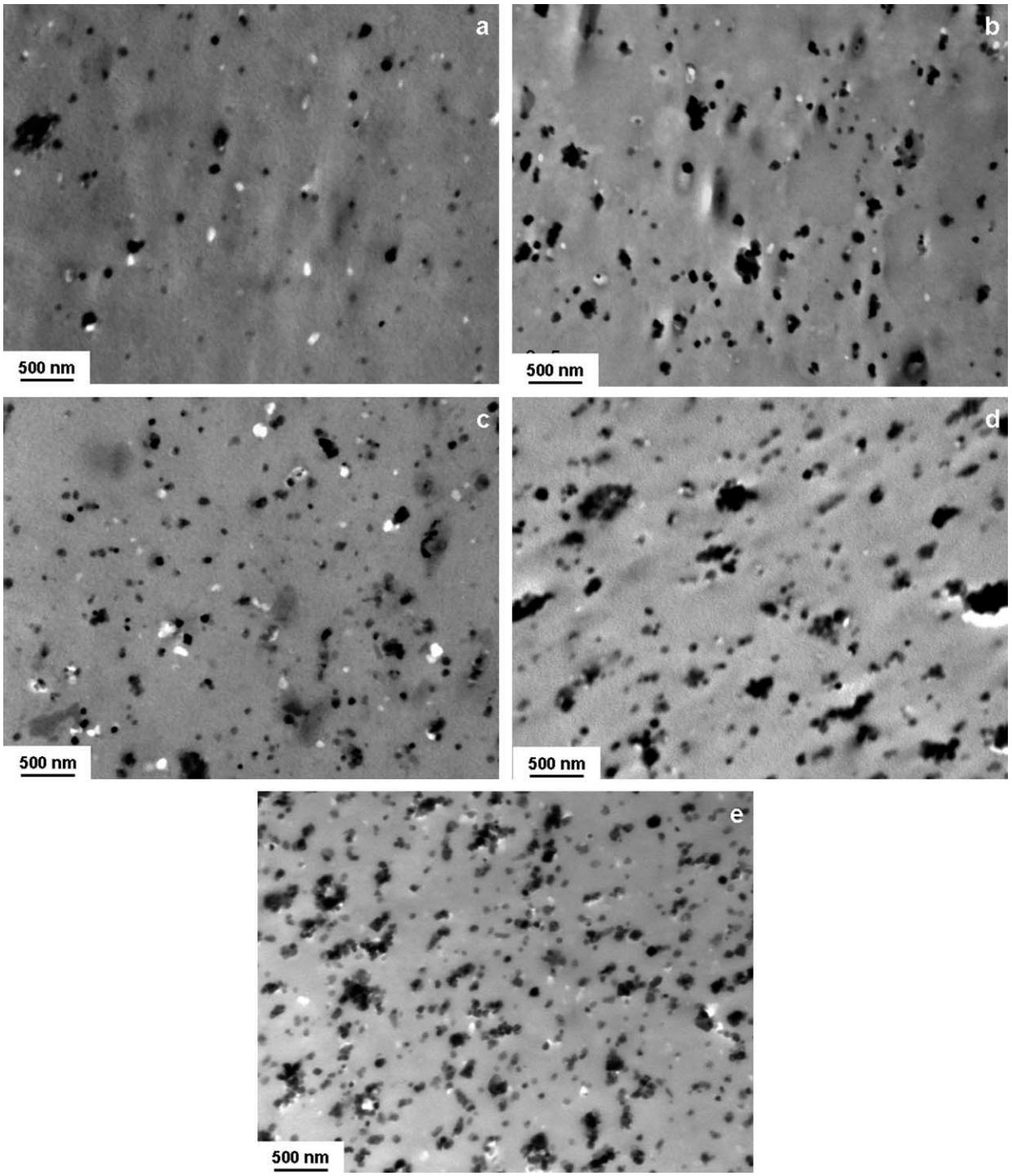

Figure 6. TEM micrograph of PVC nanocomposite with (a) 3 phr, (b) 6 phr, (c) 9 phr, (d) 12 phr, and (e) 20 phr NPCC.

particle–matrix interface strength, proposed by Vörös et al.,[26] gives the following relationship:

$$\sigma_{c,y} = \sigma_{m,y}\left(1 - \varphi_p\right) \exp \frac{\beta\varphi_p}{1 + 2.5\varphi_p}, \quad (6)$$

where $\sigma_{c,y}$ is the tensile yield strength of the composite, $\sigma_{m,y}$ is the tensile yield strength of the matrix, ϕ_p is the particle volume fraction, and β is a parameter related to the interface strength. Substitution of the experimental data into Eq. (6) gave an interfacial parameter (β) value of 1.49, which is higher than the previously recorded 1.31 for PVC nanocomposite without a coupling agent.[1] For comparison, the yield stress prediction of nanocomposites without a coupling agent was also plotted in Figure 8, based on β-value of 1.31 and taking $\sigma_m = 58$ MPa.

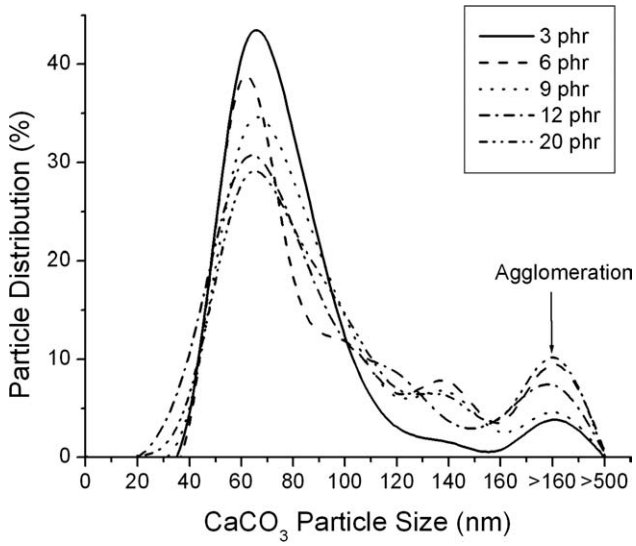

Figure 7. Image analysis on particle size distribution of PVC nanocomposites processed with titanate coupling agent.

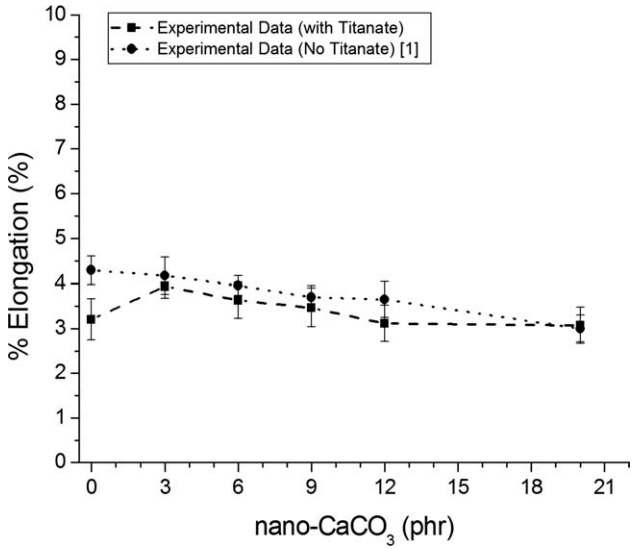

Figure 9. Effect of the NPCC content on the strain at break of PVC nanocomposites.

The interfacial parameter β was found to increase with decreasing particle size.[16] Higher β-value indicates better particle–matrix bonding, whereas weaker bonding is represented by a lower β-value.[26] The higher β-value obtained in this study supports the hypothesis that the use of a coupling agent improves the particle–matrix interfacial bond strength, which results in higher tensile strength.

Sun et al.[16] separately pretreated 80-nm $CaCO_3$ nanoparticles with titanate and reported a β-value of 1.63, indicating higher coupling efficiency when compared with the *in situ* coupling procedure used in this study. This is as expected as *ex situ* treatment would be expected to lead to better distribution of the coupling over the particle surface. In addition, the tensile yield strength of the composite exceeded the Nicolais-Narkis prediction [Eq. (7)], which is generally accepted for polymers with micron-sized particles.

$$\sigma_{c,y} = \sigma_{m,y}\left(1 - 1.21\phi_p^{2/3}\right). \quad (7)$$

The elongation at break of the PVC nanocomposites is shown in Figure 9. The strain at break increased with the addition of 3 phr NPCC reinforcement, and then gradually decreased with increasing NPCC loading up to 20 phr, where it leveled off. This observation is consistent with the observations in which no titanate was added to the matrix,[1] as with the increasing nanofiller fraction, the interfacial debonding promoted void coalescence, thereby reducing elongation at break.

Figure 10 shows increasing tensile Young's modulus of the composites with nanoparticulate volume fraction. The dynamic

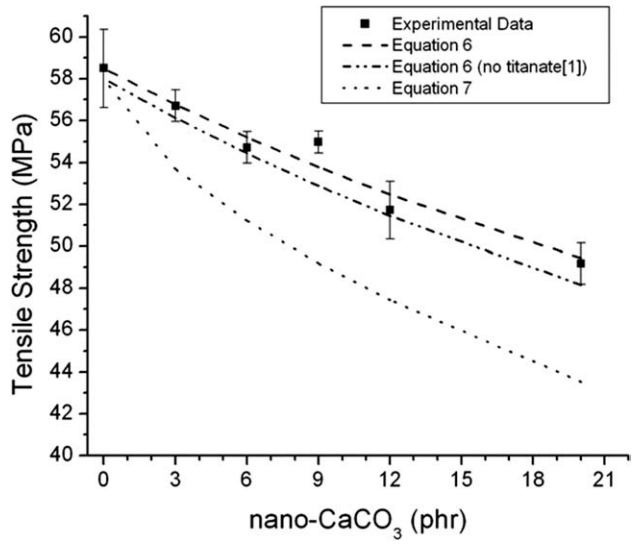

Figure 8. Effect of the NPCC content on the tensile strength of PVC nanocomposites.

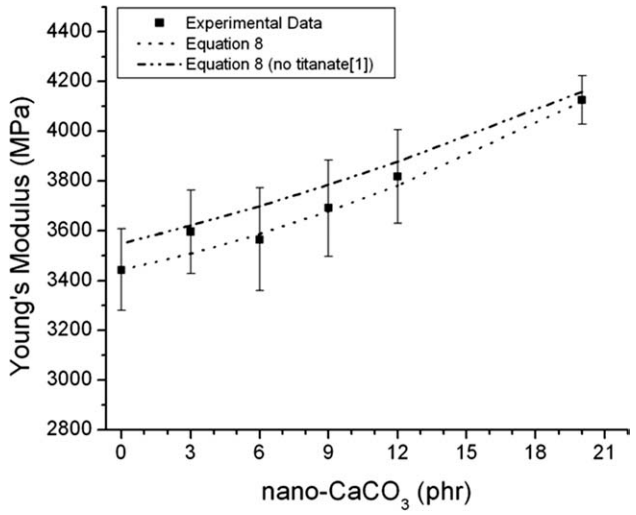

Figure 10. Effect of the NPCC content on the Young's modulus of PVC nanocomposites.

mechanical analysis test results are shown in Supporting Information Figure S3, which shows a similar trend. The increase in the modulus of rigid particulate-filled polymer composites can be well predicted by Nielsen's modified Kerner's equation, as described by Eq. (8)[27,28]:

$$E_c = E_m\left(\frac{1 + AB\phi_p}{1 - B\psi\phi_p}\right), \quad (8)$$

where E_c and E_m are the elastic moduli of the composites and the matrix, respectively. A is a constant dependent on the geometry of the filler and the Poisson's ratio of the matrix, which was calculated to be 1.25 assuming a Poisson's ratio of 0.4.[29] B is a constant dependent on the relative stiffness of the particulate filler and the matrix, which was calculated to be close to 1 due to the high filler to matrix modulus ratio. ψ is dependent on the packing fraction of the filler. Taking a packing fraction of 0.37,[30] for random close packing with agglomerates, the modulus predicted by Nielsen's modified Kerner's equation can be seen as the dotted line in Figure 10. For comparison, PVC composites without a coupling agent are also shown for the Young's modulus (Figure 10). It was found that the addition of the coupling agent can lower the modulus of the matrix and thus of the composites. This confirms the plasticizing effect of the titanate. It must be noted that the use of a coupling agent did not alter the stiffening effect due to nanoparticle reinforcement. This indicates that the degree of interfacial adhesion has a smaller effect on the modulus than does strength.

Supporting Information Figure S5 shows the Charpy impact test results indicating increasing impact energy absorbed with increasing NPCC volume fraction. The change in the Charpy impact energy is negligible for NPCC volume fractions less than 9 phr. However, PVC with 20 phr nanoparticles shows a 80% increase in the absorbed impact energy when compared with u-PVC (2 kJ/m^2). This result indicates that the use of a titanate coupling agent reduces the toughening efficiency when compared with the PVC nanocomposites without coupling agents.[1] It is hypothesized that at lower volume fractions, the 0.6 phr titanate used is sufficient to thoroughly couple the particle–matrix interface. However, this may be insufficient at higher particle volume fractions because of the increased particle–matrix interfacial area. Mechanical properties evaluation of PVC-$CaCO_3$ nanocomposite made by using *in situ* coupling with titanate coupling agent also shows similar results.[31] However, further studies are needed to confirm these results.

Figure 11 shows a similar trend in the fracture toughness or the strain energy release rate (G_c), which was ascertained from the impact tests as described by the following equation[22]:

$$G = \frac{U_s}{TW}\cdot\left(\frac{dC}{Cd\alpha}\right) = \frac{U_s}{TW\Phi(\alpha)}, \quad (9)$$

where W is the specimen width, T is the specimen thickness, and U_s is the impact energy absorbed. The calibration factor, $\Phi(\alpha)$ is a geometric term dependent on compliance, C, and the ratio of crack length over specimen width, α ($=a/W$), which is calculated using the method of Plati and Williams.[32] Plotting

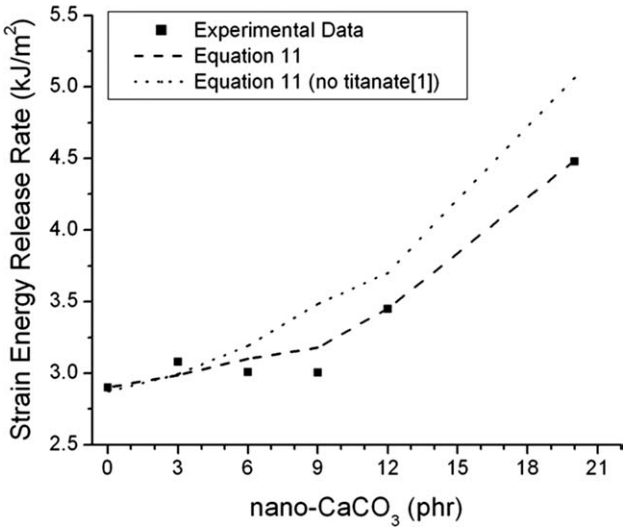

Figure 11. Effect of NPCC content on the fracture toughness (expressed as strain energy release rate) of PVC nanocomposites.

the energy lost under impact loading, U_s, divided by the cross-sectional area of the specimen, TW, versus the calibration factor, $\Phi(\alpha)$, produces a linear graph; the slope of which is G_c. Significant improvement in the fracture toughness (G_c) was recorded for nanocomposites with a NPCC filler fraction above 9 phr. At a 20 phr NPCC volume fraction, the G_c value increased from 2.89 kJ/m^2 for u-PVC to 4.48 kJ/m^2. However, when compared with PVC/nano-$CaCO_3$ composites manufactured without a coupling agent, the G_c value was lower for all filler fractions. It is believed that the titanate coupling agent promotes interfacial bonding, which inhibits cavity formation, and, hence, lowers the toughness.

FESEM images of the impact fracture surfaces show that the addition of nanoparticles alters the fracture behavior of the PVC matrix (Figure 12), whereas smooth brittle fracture characterized the monolithic PVC fracture surface [Figure 12(a)]. Nanoparticles can be seen on the fracture surfaces of the composites [Figure 12(b–f)]. The use of titanate coupling agent during melt compounding did not change the fracture characteristics of the u-PVC matrix. However, the coupling agent improved particle–matrix bonding in the composites, especially at volume fractions below 9 phr, when compared with cases where it was not incorporated [Supporting Information Figure S6(a–b)],[1] as evidenced by reduced levels of cavitation neighboring the particles. SEM analysis of the cross section of an impact fracture surface of the 9 phr composites shows no clear cavitations in the regions flanking the crack plane [Supporting Information Fig. S7(a)], especially when compared with a sample that does not contain the titanate coupling agent [Supporting Information Fig. S7(b)]. This confirms that the presence of the coupling agent promotes particle–matrix bonding, thus reducing the cavities formation, which lowers the fracture energy.[13]

Supporting Information Figure S8 shows the fracture surface of the PVC and the composites processed with the addition of a titanate coupling agent following tensile testing. The fracture surface of the titanate-containing u-PVC [Supporting Information

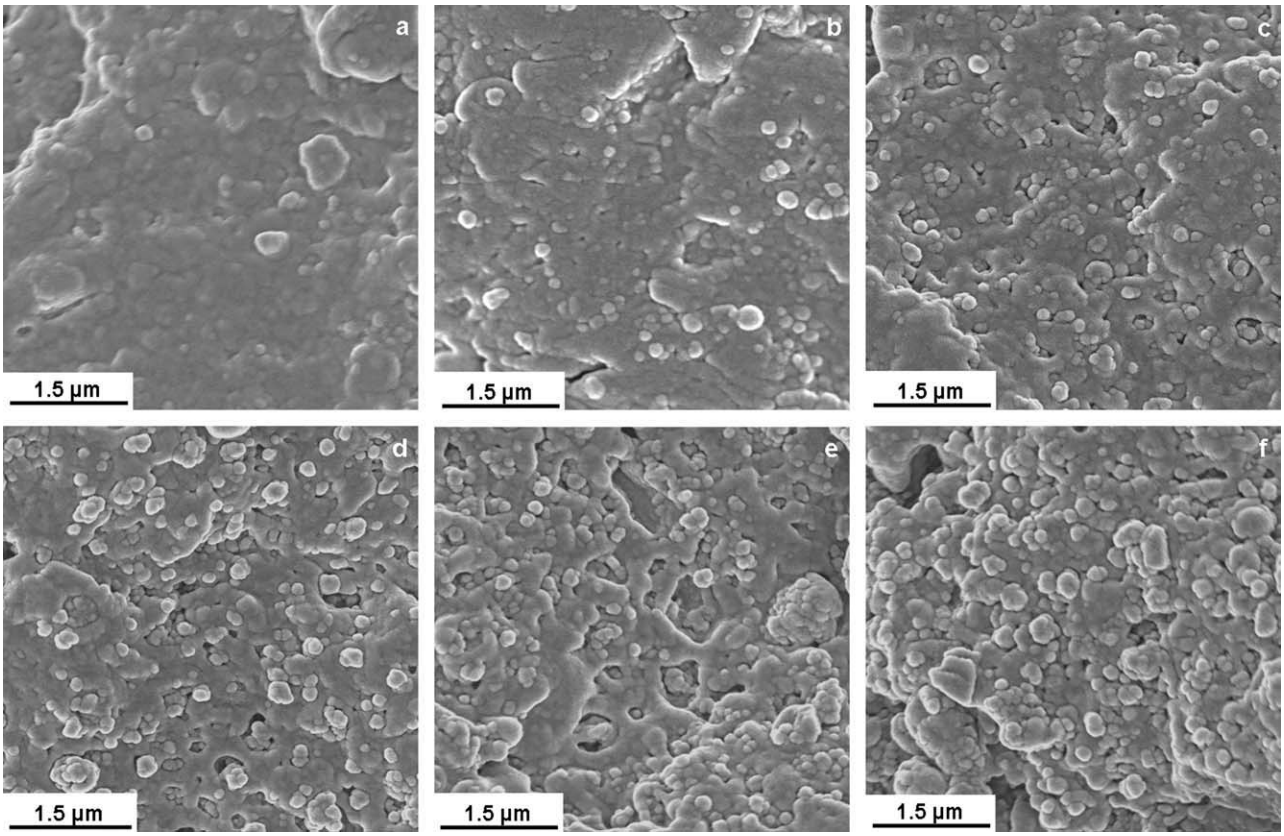

Figure 12. FESEM micrographs of the impact fracture surface of (a) u-PVC; PVC with (b) 3 phr, (c) 6 phr, (d) 9 phr, (e) 12 phr, and (f) 20 phr NPCC content.

Fig. S8(a)] shows brittle-type deformation, which is in contrast to the fibrous ductile deformation observed in u-PVC without the coupling agent.[1] However, the tensile-test fracture surfaces of the composites exhibit fibrous ductile fracture, similar to composites that did not contain the titanate [Supporting Information Fig. S8(b–f)]. The extent of fibrous structure and the number of cavities increased with the filler fraction. This indicates that without the presence of the nanoparticulate filler, the titanate may cause embrittlement in the PVC matrix.

Finite Element Analysis

Intermediate Bonding. In the case where the particles had a moderate level of bonding, it was found that the plastic deformation could proceed when the interfacial element had delaminated, noting that the debonding stress was set to be lower than or equal to the matrix yield stress. Figure 13(a) shows the contour plot of the von Mises stress at which delamination occurred—in this case at 1% applied tensile strain, indicating that the highest stress was concentrated at the top region of the particle. Similarly, Figure 13(b) shows that the maximum stress at the interfacial element occurred at the same location, indicating that delamination began at the top of the particle.

Debonding progressed with an increase of the applied displacement, and the maximum stress—initially found at the top of the particle—moved in a radial direction to the side of the particle, as shown in Figure 14(a). At a certain load, the matrix deformed plastically. The beginning of plasticity in the composite was identified by the von Mises stress in the matrix reaching the yield stress $\sigma_{m,y}$ defined by the tensile test. Figure 14(a) shows the contour plot of the von Mises stress, which suggests that the onset of plasticity was initiated at a point at $\sim 45^\circ$ to the side of the particle. Similarly, the contour plot of the von Mises stress distribution at the interface shows that the interfacial stress (normal to the interface) reaches the maximum value at the same location [Fig. 14(b)]. It can also be observed that there was no stress at the debonded interface element at the top of the particle, which confirms that the onset of delamination preceded the onset of plasticity in the composite.

With the increase in the applied tension, the plastic zone increased in size. To follow the evolution of the plastic zone for the various cases of bonding strength, the contour plots of the von Mises stress and strain were plotted for a number of loads (i.e., a number of applied strains ε_c), and the sizes of the plastic zone were determined. An example is given in Figure 15(a,b) for $\varepsilon_c = 2\%$; Figure 15(a) provides the plot of the von Mises stress, and Figure 15(b) shows the zone of von Mises plastic strain ε_m of greater or equal to 2% exhibiting an elliptical shape, which is similar to the plastic deformation region observed in the case of very weak interfacial bonding.[1] As the particle was assumed elastic in the FEA model, there is no plastic deformation in the particle, that is, the particle does not contribute to the energy absorption mechanism. Thus, the model suggested that after delamination, the plastic deformation behavior is similar to the weakly bonded case.[1]

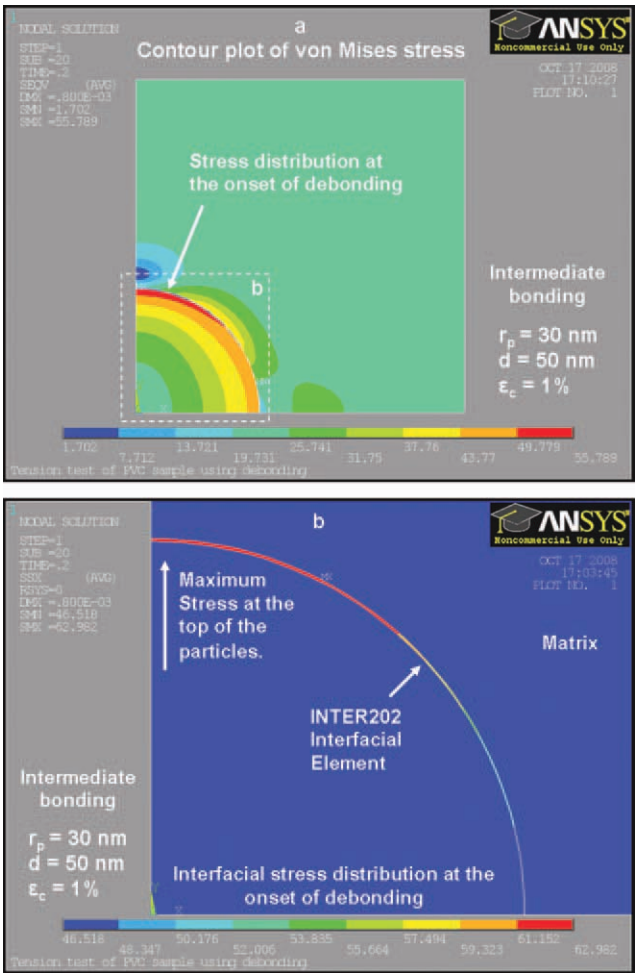

Figure 13. Contour plot of von Mises stress distribution of the (a) matrix and (b) interface at onset of debonding (ε_c = 1%) for r_p = 30 nm and d = 50 nm. [Color figure can be viewed in the online issue, which is available at wileyonlinelibrary.com.]

The applied stress on the composite at debonding ($\sigma_{c,d}$) and at matrix yielding ($\sigma_{c,p}$) as a function of particle size and spacing is depicted in Figure 16. Unlike the model with the weak bonding,[1] both stress at debonding $\sigma_{c,d}$ and stress at yielding $\sigma_{c,p}$ do not significantly change with the ratio of the interparticle distance $2d$ to particle radius r_p, that is, $2d/r_p$, as shown in Figure 16(a). Similarly, Figure 16(b) illustrates that $2d/r_p$ does not noticeably affect either the applied strain $\varepsilon_{c,d}$ at which debonding was initiated or the applied strain $\varepsilon_{c,p}$ at which plastic deformation was initiated. Instead, both the debonding and the plasticity stress and strain, that is, $\sigma_{c,d}$, $\sigma_{c,p}$, $\varepsilon_{c,d}$, and $\varepsilon_{c,p}$, significantly decreased with increasing particle radius r_p, as can be seen in Figure 16. This shows that $\sigma_{c,d}$, $\sigma_{c,p}$, $\varepsilon_{c,d}$, and $\varepsilon_{c,p}$ are dependent on particle radius r_p but independent of interparticle distance d in the range considered. The decrease of both the debonding and plasticity stress in the composite $\sigma_{c,d}$, $\sigma_{c,p}$ with increasing particle size can be associated with the fact that the larger particles are better void nucleation sites when compared with the smaller particles.[7,12,16,33–35] With increasing strain, the void coalescence eventually promotes gross yielding and failure and, hence, lowering both $\varepsilon_{c,d}$ and $\varepsilon_{c,p}$.

The dimensions of the plastic zone, that is, the horizontal radius of the ellipse r_h and the vertical radius, r_v, are shown in Figure 17(a). A comparison between r_h and r_v for weak and intermediate bonding at ε_c = 2% in Figure 17(a) shows that the size of the plastic zone was proportional to the particle size r_p and influenced by the distance to the neighboring particle d. This is consistent with previously reported results in the case of weak-bonded interface,[1] in which the proximity of the neighboring particles limits the size of the plastic zone surrounding the particle under consideration. The volume of the elliptical plastic zone with respect to the particle radius was plotted as a function of $2d/r_p$, as shown in Figure 17(b). When the debonding energy (G_{ic} = 72.2e−4 J/m^2) was lowered to 3/4 of its initial value (i.e., G_{ic} = 54.1e−4 J/m^2), there were no significant changes in the plastic zone volume [Fig. 17(b)]. Thus, as long as the particle could be debonded, the magnitude of energy required for debonding did not significantly affect the size of the plastic deformation zone around the particles. Figure 17(b)

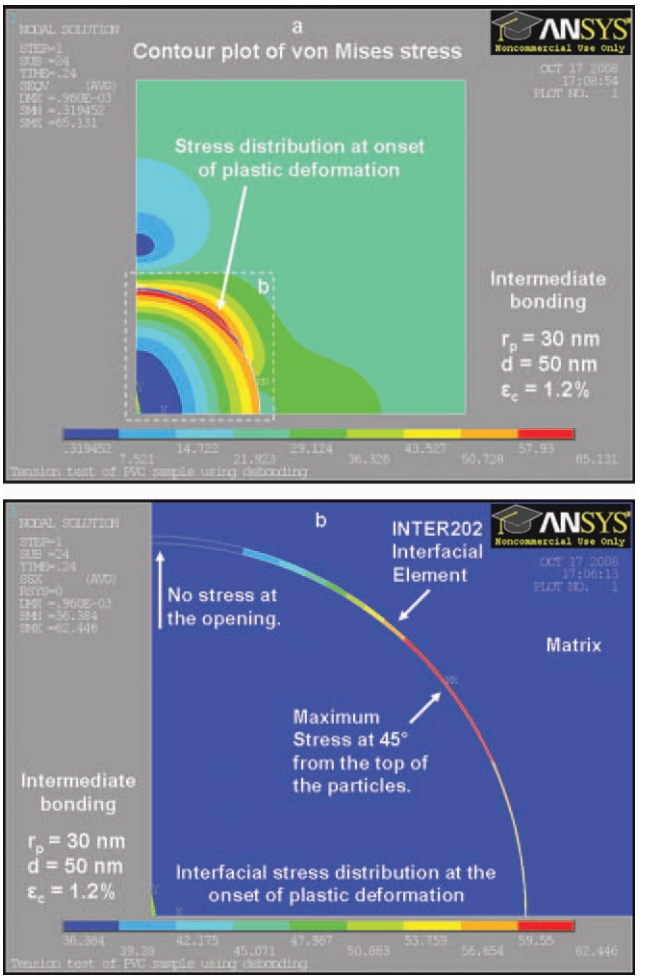

Figure 14. Contour plot of von Mises equivalent stress of the (a) matrix and (b) interface at the beginning of plasticity, where the total strain is 1.2% for r_p = 30 nm and d = 50 nm. [Color figure can be viewed in the online issue, which is available at wileyonlinelibrary.com.]

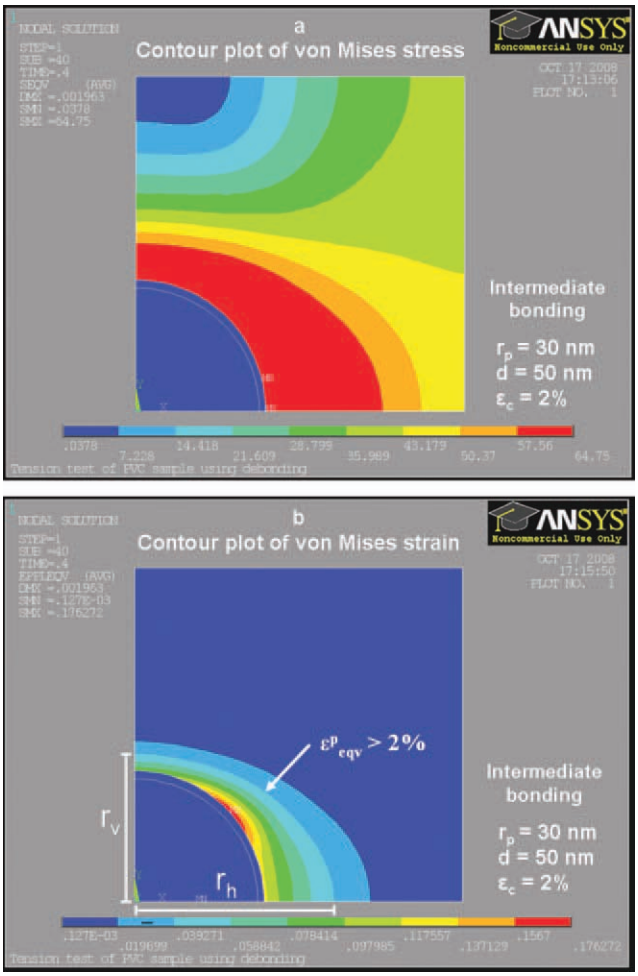

Figure 15. Contour plot of the von Mises equivalent (a) stress and (b) strain for $r_p = 30$ nm and $d = 50$ nm ($2d/r_p = 3.33$) at an applied nominal tensile strain of 2%. [Color figure can be viewed in the online issue, which is available at wileyonlinelibrary.com.]

confirms that the plastic zone size of the intermediate bonding model was slightly larger than that of the weakly bonded model.[1] This is caused by the subsequent debonding step in the intermediate bonding case and also the difference in the matrix properties, that is, the modulus of the two FE models.

Perfect Bonding. For the FEA model with perfect bonding, the contour plots of von Mises stress and strain at $\varepsilon_c = 1\%$ applied strain are shown in Figure 18. Figure 18(a) shows that the particles experience a high amount of stress, whereas the matrix experienced only a low amount of stress. Furthermore, Figure 18(b) shows a similar trend with strain; this is because of the modulus mismatch between the matrix and particles. The onset of matrix plasticity is found to occur at a higher tensile load, that is, at an applied strain of $\varepsilon_c = 2.1\%$. The contour plot of the von Mises stress shown in Figure 19(a) indicates a high stress level concentrated in the region of the matrix on the top of the particle. The evolution of the plastic zone indicates that at an applied strain (ε_c) greater than 2%, the plastic strain in the matrix ($\varepsilon_m^{eqv,p}$) first becomes >2% on the side and on the top of the particle, as shown in Figure 19(b).

Figure 20 shows that both stress and strain at the onset of plasticity increased with increasing $2d/r_p$ in the case of perfect bonding. This indicates that the onset of plasticity occurred at an applied stress higher than the monolithic matrix yield point due to increased mechanical constraint and the applied strain at the onset of plastic strain increased with $2d/r_p$.

It can be concluded that when the particles are perfectly bonded to the polymer matrix, cavity formation is suppressed. Therefore, the energy absorbed by the matrix becomes negligible at low applied strain ($\varepsilon_c = 2.1\%$), and more significant at higher strain. The rigid particles experience high levels of stress; however, fracture surface observations did not show any evidence of intraparticle fracture.

On the other hand, intermediate bonding exhibited a similar shape and size of the plastic zone with the weak-bonding model, thus allowing the energy absorption mechanism through

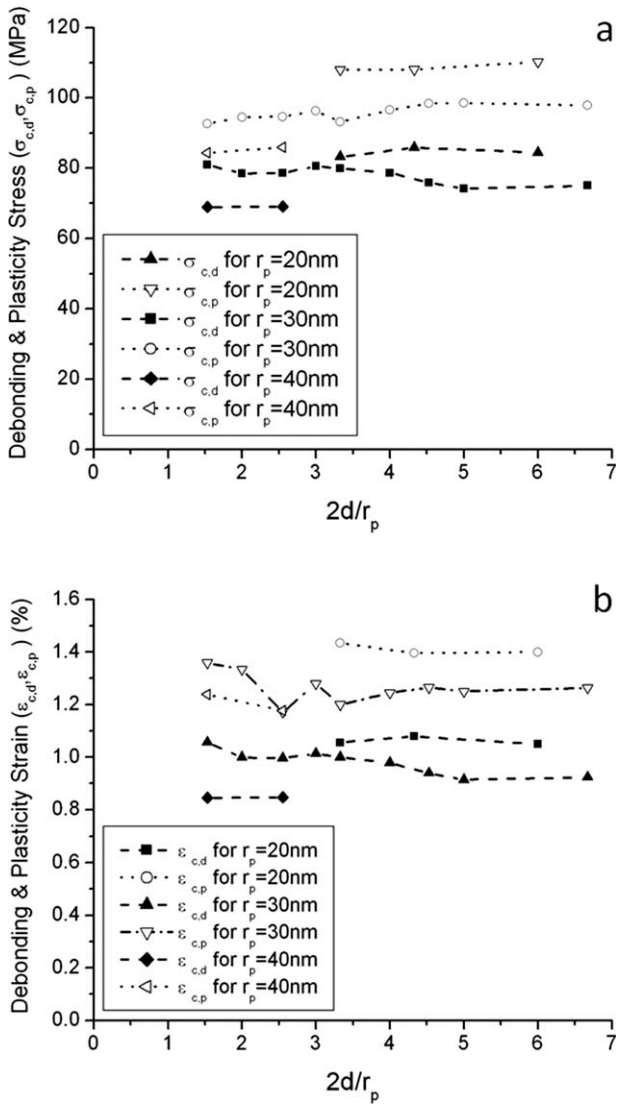

Figure 16. Variation of (a) stress and (b) strain at the onset of interface delamination and the beginning of plasticity with normalized interparticle distance.

Applied Polymer SCIENCE

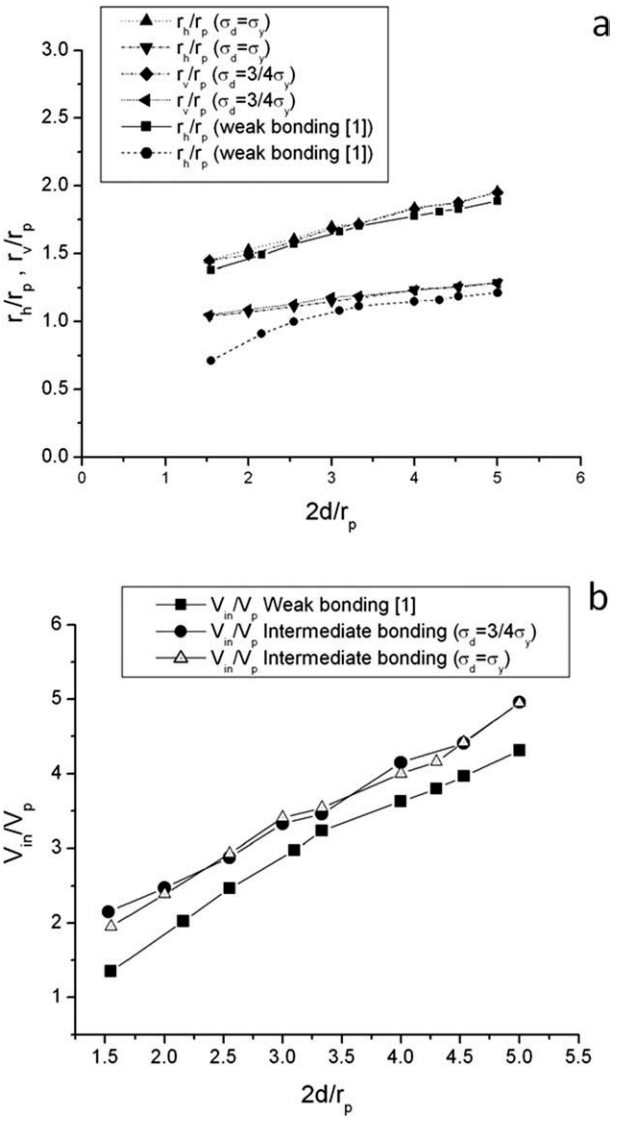

Figure 17. Variation of the (a) elliptical plastic zone radius in horizontal (r_h) and vertical (r_v) direction with normalized interparticle distance and (b) plastic zone volume with normalized interparticle distance at 2% applied tensile strain.

the inelastic deformation of the matrix around the particles. However, plasticity can occur only when debonding has occurred: intermediate bonding interface is desirable in the case where the composites need to withstand a certain amount of load before plasticity occurs. Composites with weak interfacial bonding are favorable where a toughness improvement is desired.

Fracture Mechanism

The significance of the cavitation toughening mechanism has been discussed in our previous study,[1] where the presence of nanoparticles promotes void nucleation that enhances plastic deformation and energy absorption, as illustrated in the 3D animation in the Supporting Information. The use of a 0.6 phr titanate coupling agent was found to improve particle–matrix bonding and, hence, inhibit cavity formation. In the case where the particle–matrix is perfectly bonded, it was found that cavitation is inhibited and much of the load is carried by the particles, instead of the matrix, at low strain. Hence, unless the particle fractures, energy absorption is negligible, and matrix deformation is suppressed. Plastic deformation of the matrix is possible at higher strain, in this case $\varepsilon_c \geq 2.1\%$. However, in the case of intermediate particle–matrix bonding strength, matrix plastic deformation occurs when the particle–matrix interface has delaminated. It was found that the plastic deformation zone conforms to an ellipsoidal shell around the particles with dimensions similar to those found for weak bonding.[1]

Thus, assuming moderate interfacial adhesion, the increase in the fracture energy of the PVC nanocomposites system can be predicted by multiplying the sum of interfacial fracture energy and the inelastic deformation energy with the number of particles per unit area in the process zone[25]:

$$G_{\mathrm{ic},c} = (1-\phi_f)G_{\mathrm{ic},m} + \left(\frac{3h\phi_p}{2\pi r_p^3}\right)\left(4\pi r_p^2 G_{\mathrm{ic},i} + \frac{4}{3}\pi\left(ab^2 r_p^3 - r_p^3\right)W_{\mathrm{in}}\right), \quad (10)$$

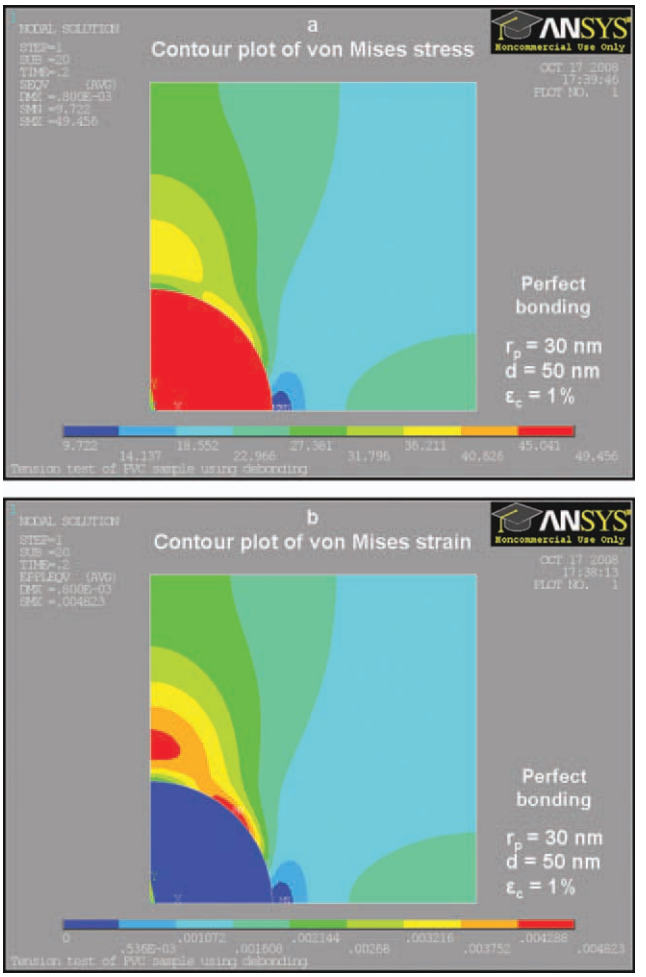

Figure 18. Contour plot of von Mises (a) equivalent stress and (b) equivalent strain at 1% applied strain for perfect bonded interface, where r_p = 30 nm and d = 50 nm. [Color figure can be viewed in the online issue, which is available at wileyonlinelibrary.com.]

where $G_{ic,m}$ is the fracture toughness of the matrix; W_{in} is the work done to inelastically deform the matrix, obtained from the area under the stress–strain curve of the matrix (Fig. 3) assuming 2% plastic strain; h is the height of the process zone calculated by Irwin approach[1]; r_p is the particle radius; and constants a and b represent the ratio of the vertical (r_v) and horizontal (r_h) semiaxes of the elliptical plastic zone with respect to the particle radius (r_p), as plotted in Figure 17(a), that is, $a = r_h/r_p$ and $b = r_v/r_p$. When Eq. (5) is substituted in Eq. (10), the fracture toughness prediction becomes:

$$G_{ic,c} = (1-\phi_f)G_{ic,m} + \left(\frac{3h\phi_p}{2\pi}\right)\left(\frac{3\sigma_{max}^2}{E_m} + \frac{4}{3}\pi(ab^2-1)W_{in}\right), \quad (11)$$

where the interparticle distance is calculated according to Ref. 35. By assuming a face-centered cubic (FCC) configuration and interfacial strength equivalent to 75% of the tensile yield stress of the matrix, the predicted strain energy release rate (G_c) is in good agreement with the experimental data, as indicated by the dashed line in Figure 11. The correlation with the FCC configuration is believed to be due to particle agglomeration, which produces an uneven particle size distribution and leads to larger particle separation than predicted by assuming simple cubic packing.[1] By substituting the parameters in Eq. (11), it was calculated that the increase in fracture energy due to interfacial debonding is between 17 and 21% for 3 phr and 20 phr particle fractions, respectively. This is slightly higher than previously found for composites with weak particle–matrix bonding where the interfacial debonding contributes to an increase in fracture energy of 10–13.5% for 3 and 20 phr, respectively.[1] The analysis shows that when there is intermediate-strength bonding between the particle–matrix, the plastic zone surrounding the particle is slightly larger when compared with the weak-bonding model.

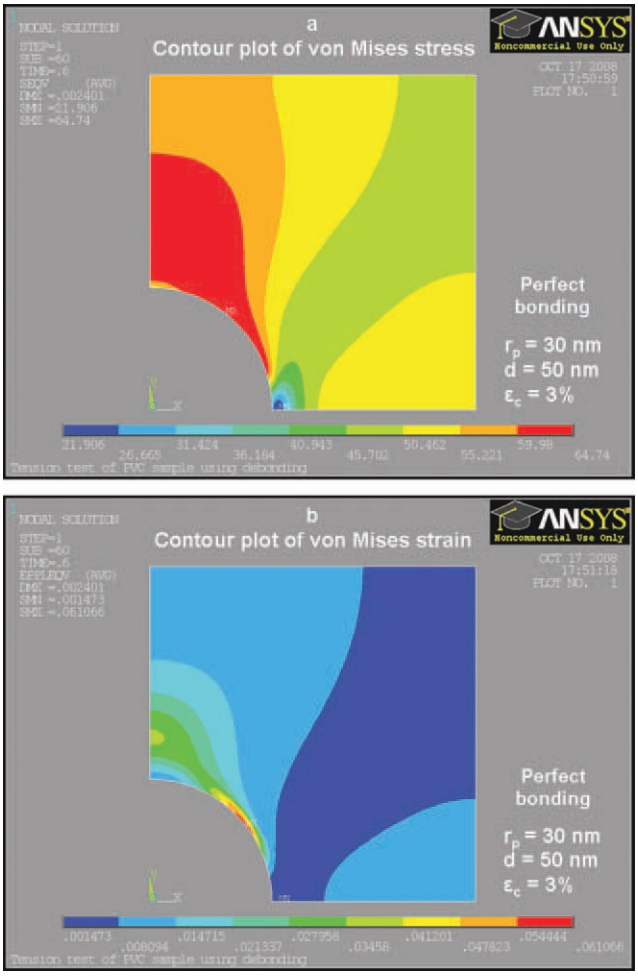

Figure 19. Contour plot of von Mises (a) equivalent stress and (b) equivalent strain at 3% applied strain (onset of plasticity) for perfect bonded interface, where $r_p = 30$ nm and $d = 50$ nm. [Color figure can be viewed in the online issue, which is available at wileyonlinelibrary.com.]

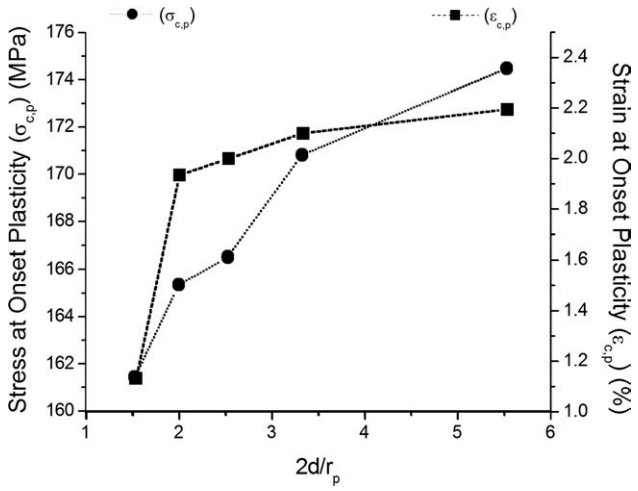

Figure 20. Variation of the stress and strain at the onset of plastic deformation with normalized interparticle distance.

However, when compared with the composites with no titanate coupling agent,[1] the fracture energy $G_{ic,c}$ of composites with titanate is generally lower. SEM micrographs of the impact fracture surface of composites with titanate generally show strong particle–matrix adhesion, and cavitation is limited when compared with composites with no coupling agent. This suggests that the *in situ* addition of titanate coupling agent leads to composites with a combined strong and intermediate interfacial bonding. In addition, it must be noted that the titanate also lowers the matrix modulus, which reduces the stiffening advantages of the nanoparticles. Thus, careful consideration must be taken when incorporating NPCC and coupling agent in PVC for engineering applications.

CONCLUSIONS

PVC nanocomposites with nanometer-sized calcium carbonate particle filler and titanate coupling agents were prepared by a melt-blending method using a two-roll mill and compression molding. It can be concluded that

1. The addition of titanate coupling agent in PVC/nano-$CaCO_3$ composites may improve particle dispersion and promote particle–matrix bonding.

2. The tensile yield strength decreases with the particle volume fraction. However, the tensile yield strength of composites processed with a coupling agent is slightly higher when compared with nanocomposites without titanate at all NPCC levels[1] because of improved particle–matrix bonding.
3. The modulus of the composite increases with the particle volume fractions following the Nielsen's modified Kerner model. However, the titanate coupling agent acts as a plasticizer and lowers the modulus of the polymer matrix, and hence, the composites processed with titanate coupling agent exhibit lower modulus when compared with nanocomposites without a coupling agent.
4. The impact energy and the fracture toughness increase with particle volume fraction. However, the impact fracture toughness of the composites with titanate is lower when compared with nanocomposites without coupling agent, especially up to 9 phr NPCC fractions.
5. FESEM observation on the impact fracture surface revealed that the nanoparticles are well bonded to the matrix due to the titanate coupling agent. This is clearly seen at 3 phr and 6 phr NPCC fractions. Thus, the addition of the coupling agent suppressed microvoids formations, which reduce the toughening effect of the NPCC.

Finite element analysis shows that

1. The von Mises equivalent stress–strain distribution in the matrix is significantly affected by the interfacial bonding strength, particle size, and interparticle distance.
2. In the case of FEA with intermediate bonding, plastic deformation of the matrix around the particle occurs when the interface has debonded. The plastic deformation zone around the particle exhibit an elliptical shape, with size dependent on the interparticle distance and particle size, similar to the weak-bonded FEA.[1]
3. In the case of strong (perfect) interfacial bonding, the rigid nanoparticles experience high amount of stress at lower strain. Plastic deformation of the surrounding matrix may occur, but at higher applied strain than that required in the case of weak and intermediate bonding.
4. Thus, when improved fracture toughness is desired, it is required that the particles are weakly bonded to the matrix that facilitates debonding and cavity formations. The use of coupling agent may improve particle dispersion and particle–matrix bonding. However, the addition of titanate coupling agent lowers the matrix modulus and inhibits cavity formation, hence, lowering the fracture toughness of the composites.

ACKNOWLEDGMENTS

The authors thank Prof. Paul Munroe, Ms. Jenny Norman, and Ms. Sigrid Fraser for assistance with the electron microscopy; Anthony Teo and Robert Podnar of Iplex Pipelines Australia Ltd. for their assistance with the sample processing; and Greg Harrison, Alex Hruza, and John Hunt of Chemson Pacific Ltd. for their assistance with the supply of polymer additives and sample processing. They also thank Singapore Nano Materials Technology for the supply of the nanoparticulate filler and Salvatore Monte of Kenrich Petrochemical Ltd. for the supply of the titanate coupling agent. They thank Felix Yakub of Vantage Interactive for the assistance in 3D animation.

REFERENCES

1. Kemal, I.; Whittle, A.; Burford, R.; Vodenitcharova, T.; Hoffman, M. *Polymer* **2009,** *50*, 4066.
2. Liu, Z. H.; Kwok, K. W.; Li, R. K. Y.; Choy, C. L. *Polymer* **2002,** *43*, 2501.
3. Chan, C. M.; Wu, J.; Li, J. X.; Cheung, Y. K. *Polymer* **2002,** *43*, 2981.
4. Markarian, J. *Plast. Additives Compounding* **2005,** *7*, 18.
5. Russel, W. B.; Saville, D. A.; Schowalter, W. R. Colloidal Dispersions; Cambridge University Press: New York, **1989.**
6. Pukánszky, B.; Fekete, E. Advances in Polymer Science; Springer: Berlin, **1999.**
7. Katz, H. S.; Milewski, J. V. Handbook of Fillers for Plastics; Springer: Berlin, **1987.**
8. Leong, Y. W.; Bakar, M. B. A.; Ishak, Z. *J. Appl. Polym. Sci.* **2005,** *98*, 413.
9. Fekete, E. A.; Pukanszky, B.; Toth, A.; Bertoti, I. *J. Colloid Interface Sci.* **1990,** *135*, 200.
10. Lutz, J. T.; Grossman, R. F. Polymer Modifiers and Additives; Marcel Dekker: New York, USA **2001.**
11. Monte, S. J.; Sugerman, G. *Polym. Eng. Sci.* **1984,** *24*, 1369.
12. Wu, D. Z.; Wang, X. D.; Song, Y. Z.; Jin, R. G. *J. Appl. Polym. Sci.* **2004,** *92*, 2714.
13. Han, C. D.; Sandford, C.; Yoo, H. J. The Annual Technical (ANTEC) Conference, Society of Plastic Engineer: New York, USA **1980.**
14. Han, C. D.; Van Den Weghe, T.; Shete, P.; Haw, J. R. *Polym. Eng. Sci.* **1981,** *21*, 196.
15. Xanthos, M. *Adv. Mater.* **2006,** *18*, 247.
16. Sun, S.; Li, C.; Zhang, L.; Du, H. L.; Burnell-Gray, J. S. *Polym. Int.* **2006,** *55*, 158.
17. Moore, D. R.; Pavan, A.; Williams, J. G.; Fracture Mechanics Testing Methods for Polymers, Adhesives, and Composites: Elsevier Science; Elsevier: Amsterdam, **2001.**
18. Monte, S. J.; Sugerman, G. Ken-React Reference Manual-Titanate and Zirconate Coupling Agents; Kenrich Petrochemicals: Bayone, NJ, **1985.**
19. ISO R527 : 1966. Plastic—Determination of Tensile Properties: International Standard Organization.
20. AS1145.1–2001. Determination of Tensile Properties of Plastic Materials: Australian Standard-Australia.
21. AS1146.2–1990. Methods for Impact Tests on Plastics—Charpy Impact Resistance: Australian Standard-Australia.
22. ISO/DIS 11673.2 : 1999. Determination of the Fracture Toughness Properties of Unplasticized Poly(vinyl chloride) (PVC-U) Pipes: International Standard Organization, **1999**.
23. Du, X. W.; Sun, G.; Nie, C. *Key Eng. Mater.* **2004,** *274*, 1077.

24. Gent, A. N. *J. Mater. Sci.* **1980,** *15*, 2884.
25. Norman, D. A.; Robertson, R. E. *Polymer* **2003,** *44*, 2351.
26. Vörös, G.; Fekete, E.; Pukánszky, B. *J. Adhes.* **1997,** *64*, 229.
27. Nielsen, L. E. *J. Polym. Sci. Polym. Phys. Ed.* **1979,** *17*, 1897.
28. Lewis, T.; Nielsen, L. *J. Appl. Polym. Sci* **1970,** *14*, 1449.
29. Erhard, G. Designing with Plastics; Hanser: Munich, Germany **2006.**
30. Vassileva, E.; Friedrich, K. *J. Appl. Polym. Sci.* **2003,** *89*, 3774.
31. Kemal, I.; Whittle, A.; Burford, R.; Vodenitcharova, T.; Hoffman, M. In Proceedings of the 69th Annual Technical Conference and Exhibition, ANTEC 2011, Society of Plastic Engineer Wiley Publishing Hoboken: New Jersey, USA, May 1–5, **2011; 743 pp.**
32. Plati, E.; Williams, J. G. *Polym. Eng. Sci.* **1975,** *15*, 470.
33. Nakamura, Y.; Fukuoka, Y.; Iida, T. *J. Appl. Polym. Sci.* **1998,** *70*, 311.
34. Mishra, S.; Perumal, G. B.; Naik, J. B. *Polym. Plast. Technol. Eng.* **1997,** *36*, 489.
35. Xie, X. L.; Liu, Q. X.; Li, R. K. Y.; Zhou, X. P.; Zhang, Q. X.; Yu, Z. Z.; Mai, Y. W. *Polymer* **2004,** *45*, 6665.